Sensors and Actuators B 223 (2016) 761–767

Contents lists available at ScienceDirect

Sensors and Actuators B: Chemical

journal homepage: www.elsevier.com/locate/snb

Enhanced toluene sensing performance of gold-functionalized $WO_3 \cdot H_2O$ nanosheets

Feng Li [a], Chao Li [a], Linghui Zhu [a], Wenbin Guo [b], Liang Shen [a], Shanpeng Wen [a,*], Shengping Ruan [b,*]

[a] State Key Laboratory on Integrated Optoelectronics, Jilin University, Changchun 130012, PR China
[b] College of Electronic Science and Engineering, Jilin University, Changchun 130012, PR China

ARTICLE INFO

Article history:
Received 9 February 2015
Received in revised form 27 July 2015
Accepted 2 October 2015
Available online 9 October 2015

Keywords:
$WO_3 \cdot H_2O$ nanosheets
Au-functionalization
Toluene
Gas sensor

ABSTRACT

Au nanoparticle-functionalized composites have been proven to be promising materials for gas sensing applications. We successfully synthesized tungsten oxide ($WO_3 \cdot H_2O$) nanosheets by a facile and effective hydrothermal process and decorated Au nanoparticles on their surface for ultra-high sensitivity levels to toluene gas. The structure and morphology of the samples were characterized by X-ray diffraction (XRD), Energy Dispersive X-ray Spectrometer (EDX), scanning electron microscopy (SEM) and transmission electron microscopy (TEM). Gas-sensing measurements revealed superior toluene sensing properties of Au nanoparticle-functionalized $WO_3 \cdot H_2O$ nanosheets (Au-$WO_3 \cdot H_2O$) compared with bare $WO_3 \cdot H_2O$. The maximum response value of Au-WO_3 reached 50–100 ppm toluene at 300 °C, which was nearly four times as high as that of bare WO_3. Meanwhile, Au-$WO_3 \cdot H_2O$ exhibited the shorter response/recovery time, better selectivity and lower operating temperature to toluene gas than those of bare $WO_3 \cdot H_2O$. Also, the mechanism involved in improving the toluene sensing properties of $WO_3 \cdot H_2O$ by Au nanoparticle-functionalization was discussed.

1. Introduction

Toluene is a common solvent used either singly or in solvent mixtures in many industrial processes. It is a colorless, volatile liquid and its vapor is flammable and explosive. The transformation of toluene in ozone in atmosphere is responsible of green-house effect. The narcotic and neurotoxic properties of toluene represent the main health hazards. High concentrations of toluene vapor may cause fatigue, weakness, confusion, dizziness, drowsiness, and unconsciousness in short-term occupational exposure. Long-term occupational exposure may result in impairment of the central nervous system. The LOAEL for effects on the central nervous system from occupational studies is approximately 88 ppm [1–4].

Due to rapid growth of industry and academia, there has been an increasing attention on fabricating high-performance sensors for hazardous and poisonous gases [5–8]. To realize ultra-high gas sensing levels which are regulated by sensitivity, selectivity, response/recovery time and stability of gas sensors, significant efforts have been made in fabrication of active sensing materials [9–12]. Among different kinds of sensing materials, including polymers, carbon nanotubes, and moisture absorbing materials, nanostructural metal oxide semiconductors are discovered to prevent possible disasters caused by harmful gases for their advantages such as low cost, controllable preparation, good selectivity and biological and chemical stability [13], desirable surface activity and high response.

Tungsten oxide (WO_3) is an indirect band gap n-type semiconductor [14] and has been intensively investigated in a variety of fields including gas sensors [15,16], electrochromic and photochromic devices [17], optical emitters [18], lithium ion batteries [19,20], photocatalysts [21,22] and solar energy devices in past decades. However, enhancing the gas sensing performance to meet the practical application requirements is still a challenge.

To further improve the gas sensing performance of metal oxide semiconductor sensors, many researchers have made tremendous efforts. It is well known that metallic catalysts such as Ag, Au, Pd, Pt nanoparticles decorated onto the surfaces of metal oxide could greatly improve gas sensing response, response/recovery speed and selectivity, and decrease the optimal operating temperature [9,23–25]. Recently, Vallejos et al. deposited gold nanoparticles onto nanostructured material WO_3 via the Aerosol Assisted Chemical Vapour Deposition (AACVD) [25]. Chávez et al. functionalized Pd particles onto the surface of WO_3 nanowires via a drop-casting method using a saturate $PdCl_2$ solution [26]. Tao He et al. deposited

* Corresponding authors.
E-mail addresses: sp_wen@jlu.edu.cn (S. Wen), ruansp@jlu.edu.cn (S. Ruan).

http://dx.doi.org/10.1016/j.snb.2015.10.005
0925-4005/

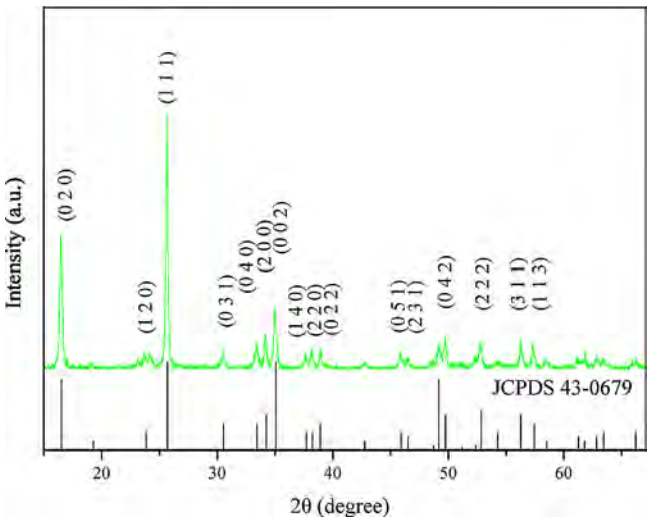

Fig. 1. XRD pattern of bare $WO_3 \cdot H_2O$.

gold nanoparticles onto the surface of a vacuum-evaporated WO_3 thin film through a spin-coating technique [27].

In this work, we successfully synthesized $WO_3 \cdot H_2O$ nanosheets by a hydrothermal method and decorated Au nanoparticles onto their surface through a facile solution process. To demonstrate the potential applications, the as-prepared materials were used to fabricate gas sensors. The measuring results revealed that the Au-functionalized $WO_3 \cdot H_2O$ nanosheets sensor exhibited higher response, faster response/recovery speed, better selectivity and lower optimum operating temperature to toluene compared with bare $WO_3 \cdot H_2O$. The possible mechanism involving in the enhanced toluene sensing properties induced by Au nanoparticles functionalization was also discussed.

2. Materials and methods

2.1. Chemical reagents

All the starting materials (AR grade): $Na_2WO_4 \cdot 2H_2O$, citric acid were purchased from the Sinopharm Chemical Reagent Co. Ltd., and no subsequent purification processes were carried out.

2.2. Preparation of gold-functionalized $WO_3 \cdot H_2O$ nanosheets

Firstly, synthetic process of $WO_3 \cdot H_2O$ was as follows: 0.5 g of $Na_2WO_4 \cdot 2H_2O$ was dissolved in 30 ml distilled water and stirred for 20 min at room temperature. Then 4 ml of 3 M HCl aqueous solution was introduced. After 10 min of stirring, 0.6 g citric acid was added. Then the resulting yellow suspension was transferred into a 50 ml Teflon-lined stainless steel autoclave, sealed and treated at 120 °C for 24 h. After the hydrothermal reaction was completed, the resulting product was washed with distilled water for three times to remove the ions, and finally dried in air at 60 °C overnight to obtain nanocrystalline $WO_3 \cdot H_2O$.

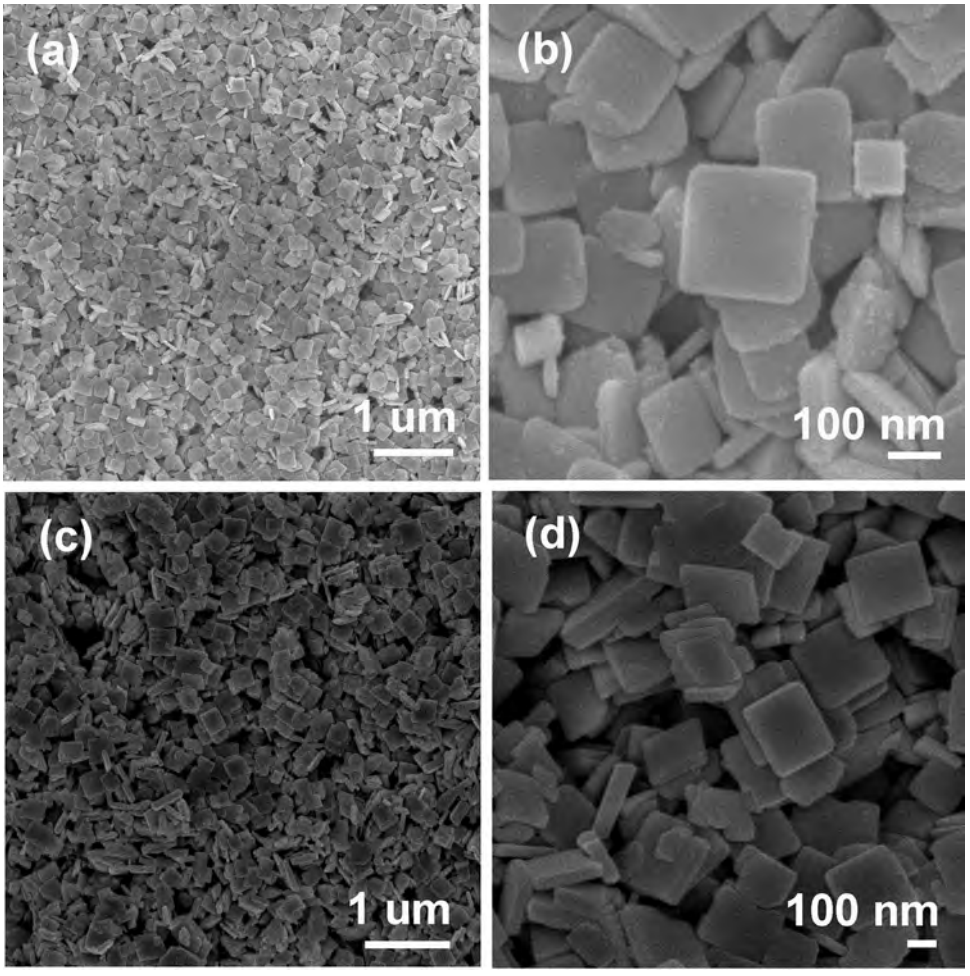

Fig. 2. SEM images of WO_3 nanostructures: (a), (b) bare $WO_3 \cdot H_2O$, (c), (d) Au nanoparticle-functionalized $WO_3 \cdot H_2O$.

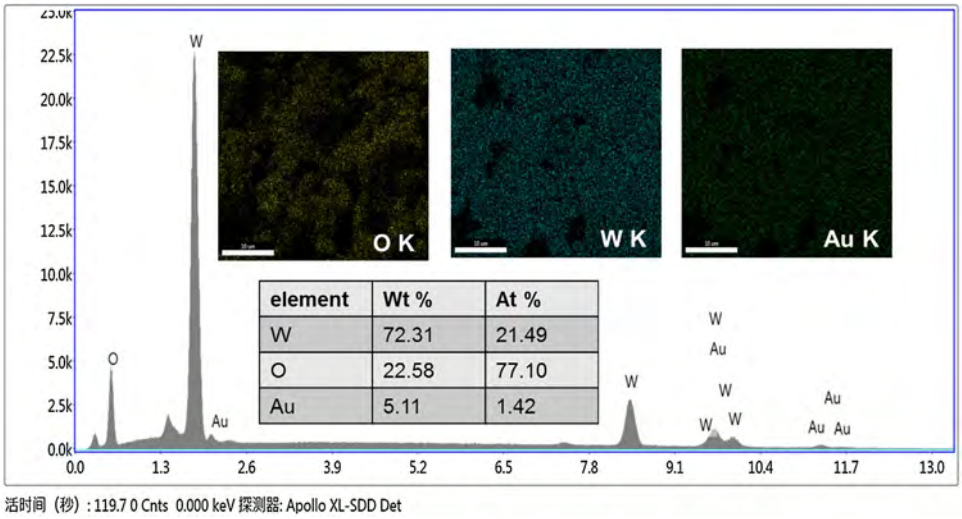

Fig. 3. EDX image of Au nanoparticle-functionalized $WO_3 \cdot H_2O$.

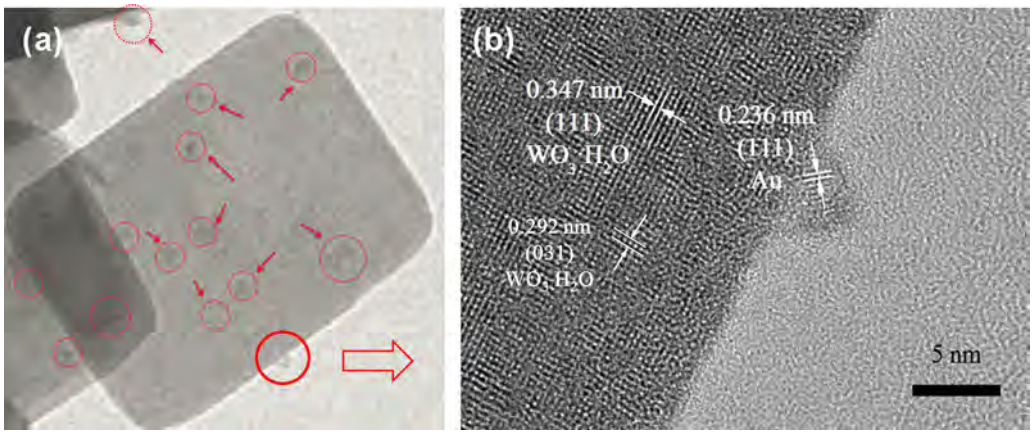

Fig. 4. (a) Typical TEM image of the Au-functionalized $WO_3 \cdot H_2O$ nanosheet, (b) HRTEM image taken from (a).

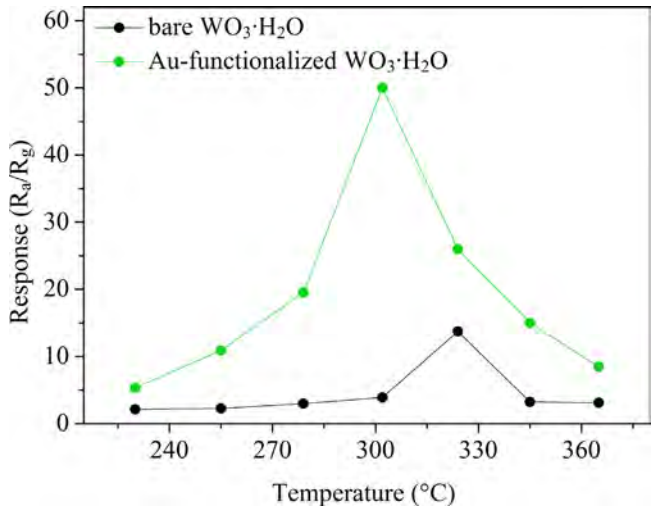

Fig. 5. Responses of sensors based on bare $WO_3 \cdot H_2O$ and Au-functionalized $WO_3 \cdot H_2O$ to 100 ppm toluene as a function of operating temperature.

Secondly, functionalization process of the $WO_3 \cdot H_2O$ nanosheets was as follow: The prepared $WO_3 \cdot H_2O$ nanosheets (0.067 g) were suspended in 20 ml distilled water. Then 0.2 ml of 0.05 M $HAuCl_4$ solution and 1 ml of 4 M NH_3 solution were added into the $WO_3 \cdot H_2O$ suspension followed by stirring for 6 h at 50 °C.

2.3. Characterization

The crystalline phase was analyzed by X-ray diffraction (XRD) using a Scintag XDS-2000 X-ray diffractometer with Cu Kα radiation (λ = 1.5418 Å). Scanning electron microscopy (SEM) images were performed on a SHIMADZU SSX-550 (Japan) instrument to observe the morphologies and sizes of the samples. Transmission electron microscope (TEM) images and Energy dispersive X-ray spectrogram (EDX) were obtained on a JEM-ARM200F.

2.4. Fabrication and measurement of sensors

The fabrication of the sensors has been reported by other groups [28,29]. The as-prepared material was mixed with deionized water in a weight ratio of 100:25 and ground in a mortar to form a paste. The paste was then coated uniformly on an Al_2O_3 ceramic tube with a couple of parallel Au electrodes (each electrode contact with two platinum wires) to form a sensing film (a thickness of about 300 μm). A Ni–Cr heating wire was placed through the alumina tube as a heater to provide an operating temperature for the gas sensor. The electrical contact was made through connecting four platinum wires and the heating wire with the sensor pedestal by welding.

Gas sensing characteristics were measured by CGS-8 intelligent gas sensing analysis system (Beijing Elite Tech Co. Ltd., China). The

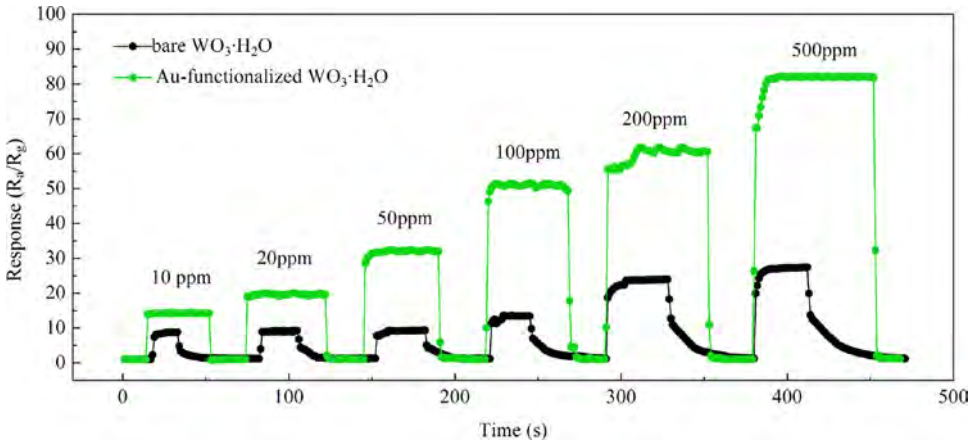

Fig. 6. Gas-sensing transients to 10–500 ppm toluene operated at optimal operating temperature.

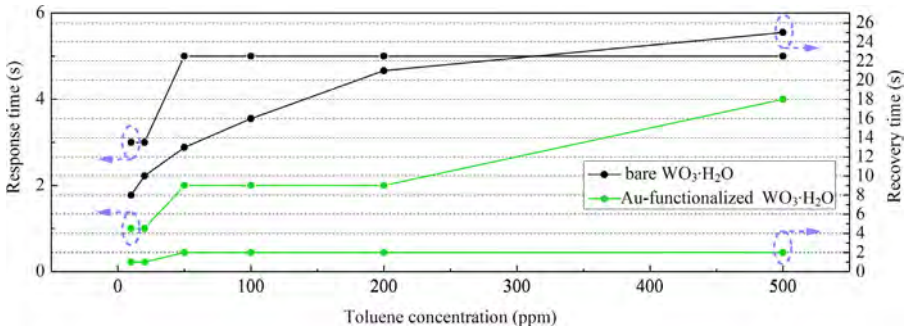

Fig. 7. Response time and recovery time of bare $WO_3·H_2O$ and Au-functionalized $WO_3·H_2O$ to 10–500 ppm toluene.

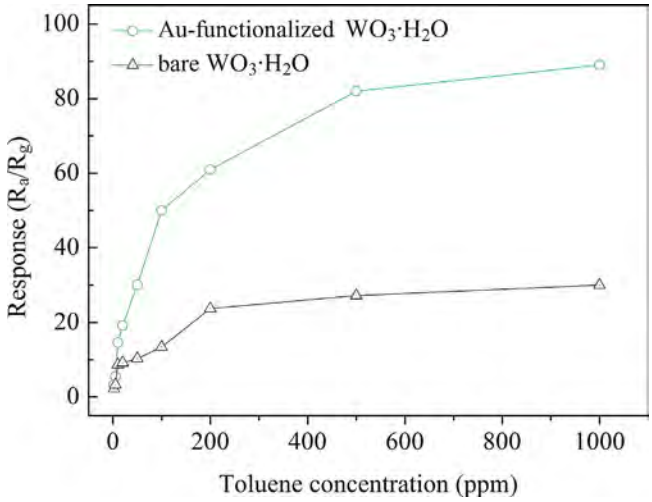

Fig. 8. Response of bare $WO_3·H_2O$ and Au-functionalized $WO_3·H_2O$ versus toluene concentrations (2–1000 ppm).

response value (S) is defined as the ratio $S = R_a/R_g$ for the reduced gas or $S = R_g/R_a$ for the oxidized gas, where the R_g and R_a are the resistance values of sensors in the presence and absence of the target gas, respectively.

3. Results and discussion

3.1. Characterization

The XRD pattern of bare $WO_3·H_2O$ was shown in Fig. 1. The XRD spectrum showed that the obtained peaks could be indexed to the (0 2 0), (1 1 1), (0 3 1), (0 4 0), (2 0 0) and (0 0 2) planes of $WO_3·H_2O$, which was in consistent with No. 46-0379 of the Joint Committee on Powder Diffraction Standards card (JCPDS). The diffraction peaks of $WO_3·H_2O$ nanosheets were sharp and intense, indicating the highly crystalline character of the samples. Moreover, no additional peaks related to impurities were observed. The broadening of the peaks could be ascribed to the small size of the nanocrystals. Combined with SEM and EDX analysis of the Au-functionalized $WO_3·H_2O$ product, it can be deduced the successful synthesis of Au-functionalized $WO_3·H_2O$ nanosheets.

The size and shape of samples were further analyzed by SEM technique. Fig. 2(a) and (c) showed the low magnification SEM images of the bare $WO_3·H_2O$ and the Au nanoparticle-functionalized $WO_3·H_2O$ representatively; (b) and (d) showed the corresponding high magnification SEM images representatively. It was observed that both products are composed of a large quantity of nanosheets distributed uniformly with a thickness of ~35 nm.

Fig. 3 showed a typical EDX spectrum of Au-functionalized $WO_3·H_2O$ which confirmed the existence of the catalytic metallic particles. The results showed that the atomic gold concentration was 1.42%.

Further detailed structural analysis of the Au-functionalized $WO_3·H_2O$ nanosheets were carried out using TEM. Fig. 4a depicts a single Au-functionalized $WO_3·H_2O$ nanosheet. It can be noted that many dark spots (partly marked by the red arrows) were dotted over the surface of nanosheet. HRTEM result confirms that the dark spots were Au nanoparticles with a lattice spacing of about 0.236 nm, corresponding to the (1 1 1) plane of Au, while the spacing between adjacent lattice planes marked was 0.347 nm and 0.292 nm, which can be indexed to the (1 1 1) plane and (0 3 1) plane of $WO_3·H_2O$ (Fig. 4b).

Table 1
Performance comparison of various gas sensors toward toluene.

	Operating temperature (°C)	Toluene (ppm)	Response (R_a/R_g)	Response time (s)	Recovery time (s)
TiO_2 Nanotubes [32]	500	20	~26	-	300
Zn-SnO_2 nanofiber [33]	360	100	9.8	5	6
TiO_2-doped flowerlike ZnO [34]	290	50	10.9	7	12
SnO_2 nanofibers [35]	350	100	6	1	5
Pd functionalized WO_3 nanofibers [36]	350	1	~6	10.9	16.1
Au-functionalized $WO_3 \cdot H_2O$ in this paper	300	100	50	2	9

3.2. Gas sensing properties

The responses of the sensors based on bare $WO_3 \cdot H_2O$ and Au-functionalized $WO_3 \cdot H_2O$ nanosheets to 100 ppm toluene (C_7H_8) at different operating temperature were tested to determine the optimum operating temperature, as shown in Fig. 5. Response of gas sensor which is significantly influenced by operating temperature can achieve the maximum value at the optimal operating temperature. When operating temperature is below the optimal operating temperature, chemical adsorption and reaction between gas molecules and chemisorbed oxygen which are related to the response of gas sensors can't obtain enough activation energies. Nevertheless continuing increasing the temperature will accelerate gas desorption and results in a decrease in response [30].

As shown in Fig. 5, Au-functionalized $WO_3 \cdot H_2O$ exhibited lower optimum operating temperature (~300 °C) compared with that of bare WO_3 (~325 °C) to toluene. The response values for both materials were 50 and 13 respectively at the corresponding temperature. It was obviously that the maximum response of Au-functionalized $WO_3 \cdot H_2O$ is nearly four times as high as that of bare $WO_3 \cdot H_2O$.

The sensing transients of bare WO_3 and Au-functionalized WO_3 sensors to 10–500 ppm toluene at corresponding optimum operating temperature were given in Fig. 6. It clearly showed that introduction of Au nanoparticles improved the sensing performance in terms of response/recovery speed and sensitivity.

When exposed to reducing gases, the resistance of the sensor decreases for an n-type semiconductor as expected. The response time (τ_{res}) is defined as the time taken from R_a to $R_a - 90\% \times (R_a - R_g)$ under the target gas environment; the recovery time (τ_{rec}) is defined as the time taken from R_g to $R_g + 90\% \times (R_a - R_g)$ in the air environment [31]. In order to facilitate the comparison and analysis, the τ_{res} and τ_{rec} values to various toluene concentrations of both samples were summarized in Fig. 7. The τ_{res} values of the Au-functionalized $WO_3 \cdot H_2O$ sensor were very short while those of the bare $WO_3 \cdot H_2O$ sensor were relatively long. It was seen that the response time of both sensors increases with the increase of toluene concentration, which could be attributed to the restriction of gas diffusion. The τ_{rec} values of the Au-functionalized $WO_3 \cdot H_2O$ sensor were also shorter than those of bare $WO_3 \cdot H_2O$ sensor in the same toluene concentration. These may be attributed to that the noble nanoparticles could improve the modulation of nano-Schottky barriers during the oxidation of toluene due to the electron mechanism.

As shown in Fig. 8, the response increased with the increase of toluene concentration. The detection limit of both sensors could reach as low as 2 ppm for toluene. The responses of bare $WO_3 \cdot H_2O$ sensor to 2–1000 ppm toluene ranged from 2.2 to 30, which ranged from 3.3 to 89 for Au-nanoparticles functionalized $WO_3 \cdot H_2O$ sensor. Table 1 presents comparisons between the gas sensing performances of the Au-functionalized $WO_3 \cdot H_2O$ and other reported results. Au-functionalized $WO_3 \cdot H_2O$ in this paper exhibited shorter response/recovery time, better selectivity and lower operating temperature compared with other materials.

Fig. 9 showed the bar graph of the responses of sensors based on bare $WO_3 \cdot H_2O$ and Au-functionalized $WO_3 \cdot H_2O$ to a variety of gases with a concentration of 100 ppm, which were tested at their optimum operating temperatures. It could be observed that the response of the Au-functionalized $WO_3 \cdot H_2O$ sensor to 100 ppm toluene at 300 °C was 50, which was higher than the responses to 100 ppm ethanol, formaldehyde, ammonia, acetone and methane. Thus, the Au-functionalized $WO_3 \cdot H_2O$ sensor had better selectivity to toluene over other gases compared with bare $WO_3 \cdot H_2O$ at optimum operating temperature.

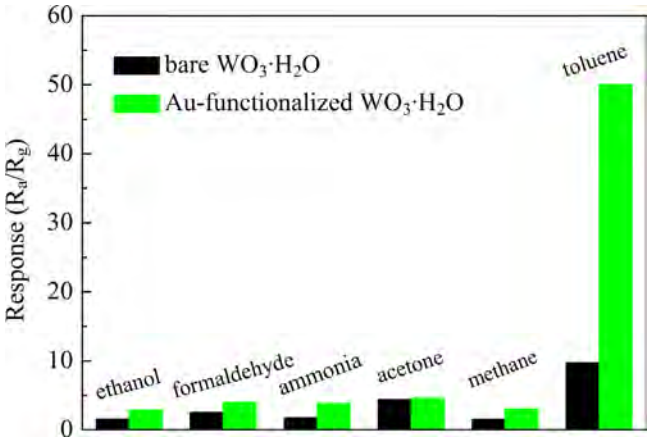

Fig. 9. Responses of the bare $WO_3 \cdot H_2O$ and Au-functionalized $WO_3 \cdot H_2O$ exposed to 100 ppm different target gases at their optimal operating temperature.

3.3. Gas sensing mechanism

WO_3 is an n-type semiconductor oxide with free electrons as the main carriers, and its sensing mechanism can be explained through the change in resistance of the sensor caused by the adsorption and desorption process of gas molecules on the surface of the gas sensing material [37]. When exposed to air at a moderate temperature, the oxygen molecules in air can form chemisorbed oxygen species (O_2^-, O^- and O^{2-}) [38] on the surface of sensing layer by capturing electrons from the conduction band of $WO_3 \cdot H_2O$ (Eqs. (1)–(4)). This brings about the formation of a thick electron-depletion region which results in the increase of the resistance of the sensors [39].

When exposed to toluene, the target gas molecules are oxidized by oxygen species and electrons are released back to the conduction band of $WO_3 \cdot H_2O$, leading to the increase of the charge carrier density, the diminish of electron depletion layer and the decrease of the resistance of the sensors. In toluene environments, target gas reacts with chemisorbed oxygen anions. These reactions can be expressed as followed (Eqs. (5)–(7)) [40,41].

$$O_{2(gas)} \rightarrow O_{2(ads)} \quad (1)$$

$$O_{2(ads)} + e^- \rightarrow O_2{}^-{}_{(ads)} \quad (T < 100\,^\circ C) \quad (2)$$

$$O_2{}^-{}_{(ads)} + e^- \rightarrow 2O^-{}_{(ads)} \quad (100\,^\circ C < T < 300\,^\circ C) \quad (3)$$

$$O^-{}_{(ads)} + e^- \rightarrow O^{2-}{}_{(ads)} \quad (T > 300\,^\circ C) \quad (4)$$

$$C_7H_8(g) \rightarrow (C_7H_8)_{ads} \quad (5)$$

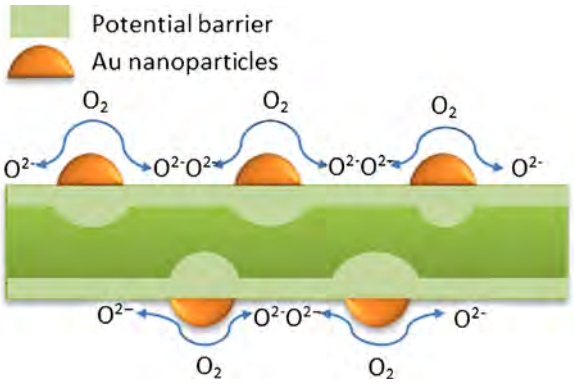

Fig. 10. Schematic diagram of the sensing mechanism of Au-functionalized $WO_3 \cdot H_2O$.

$$(C_7H_8)_{ads} + 2O^{2-}{}_{(ads)} \rightarrow C_7H_6O + H_2O + 4e^- \quad (6)$$

$$C_7H_6O + xO^{2-}{}_{(ads)} \rightarrow CO_x + H_2O(g) + 2xe^- \quad (7)$$

So, when exposed to toluene, gas molecules are absorbed on the surface of the Au functionalized $WO_3 \cdot H_2O$. Then the adsorbed toluene molecules react with chemisorbed oxygen anions, which will lead to releasing more electrons back to conduction band of bare $WO_3 \cdot H_2O$. Au functionalized-$WO_3 \cdot H_2O$ than Thus Au functionalized $WO_3 \cdot H_2O$ can generate the much larger change in the resistance, i.e. a higher response than that of bare $WO_3 \cdot H_2O$. Furthermore, for the functionalized material there are two contributions to the sensing mechanism that must also be considered. Firstly, for Au-functionalized $WO_3 \cdot H_2O$ materials, Au and $WO_3 \cdot H_2O$ would joint together to form Schottky junction, and electrons in conduction band of $WO_3 \cdot H_2O$ will transfer to Au that leads to the increase of width and height of the potential barrier. As shown in Fig. 10, the width of electron depletion layer in Au-functionalized $WO_3 \cdot H_2O$ increases which results in narrower conduction channel and less electron concentration in conduction band compared with bare $WO_3 \cdot H_2O$. So, when exposed to toluene, Au functionalized $WO_3 \cdot H_2O$ can generate the much larger change in the resistance, i.e. a higher response than that of bare $WO_3 \cdot H_2O$.

Secondly, the enhanced toluene sensing properties may be attributed to Au catalysis. As we know the enthalpy change of the dehydrogenation of the target gas is an important factor that determines the gas sensing performance [42]. When toluene gas molecules are oxidized, they are dehydrogenated first. Lower enthalpy change of the dehydrogenation possibly leads to higher response. Au nanoparticles can lower the operating temperature as a catalyst by decreasing activity energy, and accelerate the sensing reaction (Eq. (6)). So we deduce that Au nanoparticles as catalyst decreasing activity energy may be the reason for higher sensitivity, faster response/recovery speed and lower optimal operating temperature to toluene.

4. Conclusions

In summary, the bare $WO_3 \cdot H_2O$ and Au-functionalized $WO_3 \cdot H_2O$ were successfully synthesized and their toluene sensing properties were investigated. The detection limit of the Au-functionalized $WO_3 \cdot H_2O$ sensor could reach as low as 2 ppm for toluene at 300 °C. The sensors based on Au-functionalized $WO_3 \cdot H_2O$ nanosheets had a higher sensitivity, lower optimal operating temperature, faster response/recovery speed and better selectivity to toluene compared with the bare $WO_3 \cdot H_2O$ sensors. The excellent gas sensing performance of Au-functionalized $WO_3 \cdot H_2O$ sensor might be attribute to the synergistic effects of catalysis of Au nanoparticles and the presence of Au/$WO_3 \cdot H_2O$ Schottky junction. The results certified that the Au-functionalized $WO_3 \cdot H_2O$ nanosheets sensor is a potential candidate for high performance toluene sensor.

Acknowledgements

The authors are grateful to National Natural Science Foundation of China (Grant No. 61274068, 61370046, 51303061), the National High Technology Research and Development Program of China (Grant No. 2013AA030902), Project of Science and Technology Development Plan of Jilin Province (Grant Nos. 20130206021GX, 20140204056GX), and Project of Science and Technology Plan of Changchun City (Grant No. 13KG49, 14KG020, 14KG019).

References

[1] W.H. Organization, Recommended Health-Based Limits in Occupational Exposure to Selected Organic Solvents: (Report of a WHO Study Group [meeting held in Geneva from 17 to 23 June 1980], (1981)).
[2] T.P. Ng, S. Foo, T. Yoong, Risk of spontaneous abortion in workers exposed to toluene, Br. J. Ind. Med. 49 (1992) 804–808.
[3] W.H. Organization, Regional Office for Europe, Air Quality Guidelines (second ed.) WHO, Copenhagen, Denmark (2000).
[4] NIOSH, Occupational health guidelines for toluent: US Department of Health and Human Services, Public Health Service, Centers for Disease Control, National Institute for Occupational Safety and Health: US Department of Labor, Occupational Safety and Health Administration, publication no. 81-123 (1978).
[5] M. Mittal, A. Kumar, Carbon nanotube (CNT) gas sensors for emissions from fossil fuel burning, Sens. Actuators B: Chem. 203 (2014) 349–362.
[6] Q. Xiang, G. Meng, H. Zhao, Y. Zhang, H. Li, W. Ma, et al., Au nanoparticle modified WO_3 nanorods with their enhanced properties for photocatalysis and gas sensing, J. Phys. Chem. C 114 (2010) 2049–2055.
[7] J. Kim, C.W. Lee, W. Choi, Platinized WO_3 as an environmental photocatalyst that generates OH radicals under visible light, Environ. Sci. Technol. 44 (2010) 6849–6854.
[8] G. Shen, P.-C. Chen, K. Ryu, C. Zhou, Devices and chemical sensing applications of metal oxide nanowires, J. Mater. Chem. 19 (2009) 828–839.
[9] J.Y. Leng, X.J. Xu, N. Lv, H.T. Fan, T. Zhang, Synthesis and gas-sensing characteristics of WO_3 nanofibers via electrospinning, J. Colloid Interface Sci. 356 (2011) 54–57.
[10] J. Kong, N.R. Franklin, C. Zhou, M.G. Chapline, S. Peng, K. Cho, et al., Nanotube molecular wires as chemical sensors, Science 287 (2000) 622–625.
[11] W. Göpel, K.D. Schierbaum, SnO_2 sensors: current status and future prospects, Sens. Actuators B: Chem. 26 (1995) 1–12.
[12] F. Qu, Y. Wang, Y. Wang, J. Zhou, S. Ruan, Template-free synthesis of Cu_2O–Co_3O_4 core–shell composites and their application in gas sensing, RSC Adv. 4 (2014) 24211–24216.
[13] X. Hu, G. Li, J.C. Yu, Design, fabrication, and modification of nanostructured semiconductor materials for environmental and energy applications, Langmuir 26 (2009) 3031–3039.
[14] J. Su, L. Guo, N. Bao, C.A. Grimes, Nanostructured WO_3/$BiVO_4$ heterojunction films for efficient photoelectrochemical water splitting, Nano Letters 11 (2011) 1928–1933.
[15] S. Bai, K. Zhang, R. Luo, D. Li, A. Chen, C.C. Liu, Low-temperature hydrothermal synthesis of WO_3 nanorods and their sensing properties for NO_2, J. Mater. Chem. 22 (2012) 12643–12650.
[16] S. Srivastava, K. Jain, V.N. Singh, S. Singh, N. Vijayan, N. Dilawar, et al., Faster response of NO_2 sensing in graphene-WO_3 nanocomposites, Nanotechnology 23 (2012) 205501–205509.
[17] Z. Xie, Y. Zhu, J. Xu, H. Huang, D. Chen, G. Shen, Porous WO_3 with enhanced photocatalytic and selective gas sensing properties, CrystEngComm 13 (2011) 6393–6398.
[18] K. Hong, K. Kim, S. Kim, I. Lee, H. Cho, S. Yoo, et al., Optical properties of WO_3/Ag/WO_3 multilayer as transparent cathode in top-emitting organic light emitting diodes, J. Phys. Chem. C 115 (2011) 3453–3459.
[19] W.-J. Li, Z.-W. Fu, Nanostructured WO_3 thin film as a new anode material for lithium-ion batteries, Appl. Surf. Sci. 256 (2010) 2447–2452.
[20] K. Huang, Q. Pan, F. Yang, S. Ni, X. Wei, D. He, Controllable synthesis of hexagonal WO_3 nanostructures and their application in lithium batteries, J. Phys. D: Appl. Phys. 41 (2008) 155417–155423.
[21] J. Georgieva, TiO_2/WO_3 photoanodes with enhanced photocatalytic activity for air treatment in a polymer electrolyte cell, J. Solid State Electrochem. 16 (2012) 1111–1119.
[22] S. Nishimoto, T. Mano, Y. Kameshima, M. Miyake, Photocatalytic water treatment over WO_3 under visible light irradiation combined with ozonation, Chem. Phys. Lett. 500 (2010) 86–89.
[23] H.-Y. Lai, C.-H. Chen, Highly sensitive room-temperature CO gas sensors: Pt and Pd nanoparticle-decorated In_2O_3 flower-like nanobundles, J. Mater. Chem. 22 (2012) 13204–13208.

[24] Y.-C. Pu, Y.-C. Chen, Y.-J. Hsu, Au-decorated $Na_xH_{2-x}Ti_3O_7$ nanobelts exhibiting remarkable photocatalytic properties under visible-light illumination, Appl. Catal. B: Environ. 97 (2010) 389–397.
[25] S. Vallejos, T. Stoycheva, P. Umek, C. Navio, R. Snyders, C. Bittencourt, et al., Au nanoparticle-functionalised WO_3 nanoneedles and their application in high sensitivity gas sensor devices, Chem. Commun. 47 (2011) 565–567.
[26] F. Chávez, G.F. Pérez-Sánchez, O. Goiz, P. Zaca-Morán, R. Peña-Sierra, A. Morales-Acevedo, et al., Sensing performance of palladium-functionalized WO_3 nanowires by a drop-casting method, Appl. Surf. Sci. 275 (2013) 28–35.
[27] T. He, Y. Ma, Y.-a. Cao, W.-s. Yang, J.-n. Yao, Improved photochromism of WO_3 thin films by addition of Au nanoparticles, Phys. Chem. Chem. Phys. 4 (2002) 1637–1639.
[28] X. Li, W. Feng, Y. Xiao, P. Sun, X. Hu, K. Shimanoe, et al., Hollow zinc oxide microspheres functionalized by Au nanoparticles for gas sensors, RSC Adv. 4 (2014) 28005–280010.
[29] X. Li, X. Zhou, Y. Liu, P. Sun, K. Shimanoe, N. Yamazoe, et al., Microwave hydrothermal synthesis and gas sensing application of porous ZnO core–shell microstructures, RSC Adv. 4 (2014) 32538–32543.
[30] S. Bai, K. Zhang, X. Shu, S. Chen, R. Luo, D. Li, et al., Carboxyl-directed hydrothermal synthesis of WO_3 nanostructures and their morphology-dependent gas-sensing properties, CrystEngComm 16 (2014) 10210–10217.
[31] L. Wang, J. Deng, Z. Lou, T. Zhang, Cross-linked p-type Co_3O_4 octahedral nanoparticles in 1D n-type TiO_2 nanofibers for high-performance sensing devices, J. Mater. Chem. A 2 (2014) 10022–10028.
[32] M.-H. Seo, M. Yuasa, T. Kida, J.-S. Huh, K. Shimanoe, N. Yamazoe, Gas sensing characteristics and porosity control of nanostructured films composed of TiO_2 nanotubes, Sens. Actuators B: Chem. 137 (2009) 513–520.
[33] X. Song, D. Zhang, M. Fan, A novel toluene sensor based on ZnO–SnO_2 nanofiber web, Appl. Surf. Sci. 255 (2009) 7343–7347.
[34] Y. Zeng, T. Zhang, L. Wang, M. Kang, H. Fan, R. Wang, et al., Enhanced toluene sensing characteristics of TiO_2-doped flowerlike ZnO nanostructures, Sens. Actuators B: Chem. 140 (2009) 73–78.
[35] Q. Qi, T. Zhang, L. Liu, X. Zheng, Synthesis and toluene sensing properties of SnO_2 nanofibers, Sens. Actuators B: Chem. 137 (2009) 471–475.
[36] N.-H. Kim, S.-J. Choi, D.-J. Yang, J. Bae, J. Park, I.-D. Kim, Highly sensitive and selective hydrogen sulfide and toluene sensors using Pd functionalized WO_3 nanofibers for potential diagnosis of halitosis and lung cancer, Sens. Actuators B: Chem. 193 (2014) 574–581.
[37] C.W. Na, H.S. Woo, I.D. Kim, J.H. Lee, Selective detection of NO_2 and C_2H_5OH using a Co_3O_4-decorated ZnO nanowire network sensor, Chem. Commun. 47 (2011) 5148–5150.
[38] X. An, J.C. Yu, Y. Wang, Y. Hu, X. Yu, G. Zhang, WO_3 nanorods/graphene nanocomposites for high-efficiency visible-light-driven photocatalysis and NO_2 gas sensing, J. Mater. Chem. 22 (2012) 8525–8531.
[39] G. Xi, J. Ye, Synthesis of bismuth vanadate nanoplates with exposed {001} facets and enhanced visible-light photocatalytic properties, Chem. Commun. 46 (2010) 1893–1895.
[40] N. Han, H. Liu, X. Wu, D. Li, L. Chai, Y. Chen, Pure and Sn-, Ga- and Mn-doped ZnO gas sensors working at different temperatures for formaldehyde, humidity, NH_3, toluene and CO, Appl. Phys. A 104 (2011) 627–633.
[41] J. Huang, X. Xu, C. Gu, M. Yang, M. Yang, J. Liu, Large-scale synthesis of hydrated tungsten oxide 3D architectures by a simple chemical solution route and their gas-sensing properties, J. Mater. Chem. 21 (2011) 13283–13289.
[42] D. Baulch, C. Bowman, C. Cobos, R. Cox, T. Just, J. Kerr, et al., Evaluated kinetic data for combustion modeling: supplement II, J. Phys. Chem. Ref. Data 34 (2005) 757–1397.

Biographies

Feng Li received the bachelor degree in electronic science and technology from Jilin University, China in 2014. She is currently an undergraduate and interested in nanomaterials and chemical sensors.

Chao Li received the bachelor degree in electronic science and technology from Jilin University, China in 2011. Now he is working for a doctor's degree and is mainly devoted to the research of functional nanomaterials and chemical sensors.

Linghui Zhu received the bachelor degree from the College of Electronic Science and Engineering, Jilin University, China in 2011. She is currently studying for a doctor's degree and is mainly devoted to the research of functional nanomaterials, chemical sensors and photodetector.

Wenbin Guo received the PhD degree in 2004. Now, he is a professor in College of Electronics Science and Engineering, Jilin University, and mainly devoted to the research of electronic functional materials and solar cells.

Liang Shen received the PhD degree in 2009. Now, he is an associate professor in College of Electronics Science and Engineering, Jilin University, and mainly devoted to material synthesis and polymer solar cells.

Shanpeng Wen received the PhD degree in the field of Polymer Chemical and Physics, Jilin University, China in 2009. Now, he is a lecturer in College of Electronics Science and Engineering, Jilin University, and mainly devoted to the research of organic material synthesis and polymeric solar cell.

Shengping Ruan received the PhD degree of electronic science and engineering from Jilin University in 2001. Now, he is a full professor in the College of Electronics Science and Engineering, Jilin University, and mainly devoted to the research of electronic functional materials and devices.